

JGR Space Physics

RESEARCH ARTICLE

10.1029/2021JA030239

Key Points:

- Anticorrelation between tidal winds and solar cycle activity
- Anticorrelation between sporadic E (Es) layer occurrence and solar cycle
- Evidence of solar wind high speed streams influence in the mesosphere lower thermosphere (MLT) region winds

Correspondence to:

V. F. Andrioli,
vania.andrioli@inpe.br

Citation:

Andrioli, V. F., Xu, J., Batista, P. P., Resende, L. C. A., Da Silva, L. A., Marchezi, J. P., et al. (2022). New findings relating tidal variability and solar activity in the low latitude MLT region. *Journal of Geophysical Research: Space Physics*, 127, e2021JA030239. <https://doi.org/10.1029/2021JA030239>











Received 21 DEC 2021

Accepted 28 FEB 2022

Author Contributions:

Funding acquisition: C. Wang
Investigation: L. C. A. Resende, L. A. Da Silva
Methodology: A. Guharay
Project Administration: Z. Liu
Supervision: J. Xu, P. P. Batista, H. Li

New Findings Relating Tidal Variability and Solar Activity in the Low Latitude MLT Region

V. F. Andrioli^{1,2,3} , J. Xu¹ , P. P. Batista³ , L. C. A. Resende^{1,2,3} , L. A. Da Silva^{1,2,3} , J. P. Marchezi^{1,2,3} , H. Li¹ , C. Wang¹ , Z. Liu^{1,2} , and A. Guharay⁴ 

¹State Key Laboratory of Space Weather—NSSC/CAS, Beijing, China, ²China-Brazil Joint Laboratory for Space Weather, NSSC/INPE, São José dos Campos, Brazil, ³National Institute for Space Research (INPE), São José dos Campos, Brazil, ⁴Physical Research Laboratory, Ahmedabad, India

Abstract Mesospheric winds have been measured by meteor radar at Cachoeira Paulista (22.7°S; 45°W) since April 1999. The tidal components were analyzed over about 21 years of available data exhibiting an annual and semi-annual variation. Amplitudes of meridional diurnal (semidiurnal) tide are on averaged 30% (28%) and the zonal ones are 14% (20%) stronger at solar minimum than at solar maximum. The anticorrelation between F10.7 cm solar flux and amplitudes of the semiannual oscillation of diurnal and semidiurnal tides is presented. Additionally, the sporadic E (Es) layers occurrence has an anti-correlation with solar activity due to the tidal wind variation. A discussion about the physical mechanism is performed in terms of the particle precipitation during High-Speed Stream (HSS) events according to the solar cycle. Finally, a superposed epoch analysis of the tidal amplitudes during the HSS events in 2018 is presented. And a slight increase in all tidal components is seen when the structure reached the Earth and in the following days showing that indeed the electron precipitation during HSS events affect the tidal amplitudes.

1. Introduction

Solar tides constitute the dominant components of the motion field in the mesosphere-lower-thermosphere (MLT) region at low latitudes. Both theoretical and experimental studies have shown the presence of a semi-annual oscillation (SAO) in the diurnal and semidiurnal tidal fields (see Hagan et al., 1999; Hagan & Forbes, 2002 for theoretical studies and Andrioli et al., 2009; Batista et al., 2004; Burrage et al., 1995; Huang & Reber, 2003; Reddi & Ramkumar, 1997 for observations). In addition, some studies have also revealed variability occurring on time scales ranging from a few days (e.g., Fritts & Isler, 1994; Nakamura et al., 1997) to the long-term. The latter includes annual, 11-year solar-cycle, and quasi-biennial oscillations (e.g., Araújo et al., 2020; Deepa et al., 2008; Guharay et al., 2019; Gurubaran & Rajaram, 1999; Iimura et al., 2010; Vincent et al., 1998).

Atmospheric tides are excited by the absorption of ultraviolet radiation by ozone in the stratosphere-mesosphere and radiation in the Schumann–Runge bands and continuum by molecular oxygen and nitrogen in the lower thermosphere, in addition to the absorption of infrared radiation by tropospheric water vapor (Forbes & Garrett, 1979). The solar cycle is expected to influence solar tides since the ultraviolet radiation changes with solar activity. Some studies have been made concerning the long-term variation of atmospheric fields related to solar activity (e.g., Clemesha et al., 2005; Dickinson, 1975; Fuller-Rowell & Rees, 1980; Mohankumar, 1985). Focusing on tidal winds, most of these studies have tried to identify the relation between tides and solar activity (e.g., Deepa et al., 2008; Guharay et al., 2019; Iimura et al., 2010; Pancheva et al., 2003). Iimura et al. (2010) correlated the 11-year solar cycle with the diurnal tide amplitude and found an anti-phase relationship between them. Yi, Reid, Xue, Younger, Murphy, et al. (2017) and Yi, Reid, Xue, Younger, Spargo, et al. (2017) showed evidence of mesospheric density responses to the solar wind High Speed Stream (HSS), and an anticorrelation was seen with the geomagnetic indexes Kp and AE. Guharay et al. (2019) studied the relation between seasonal amplitudes of tides with the solar cycle and also observed an anti-phase association mainly in the equinoxes. Although these authors presented several results showing the anticorrelation between geomagnetic activity and the response observed in mesosphere lower thermosphere (MLT) region, there is still no convincing explanation for this coupling.

The tidal and prevailing winds in the MLT region over Cachoeira Paulista (CP, 22.7°S; 45°W) were extensively analyzed by Batista et al. (2004). As predicted by theory, the diurnal component was found to be dominant, and the SAO shows some inter-annual variability. Additionally, for the semidiurnal tide, they observed a more

complex behavior in SAO. Furthermore, much of the inter-annual variability in mean and tidal winds remains unexplained at present.

Tidal winds have an important role in the development of Sporadic layers in the ionospheric E region across different regions of the globe (Luo et al., 2021; Resende et al., 2017a, 2017b, 2021). These layers are characterized by patches of enhanced electron density around 95–140 km in the ionosphere, composed mainly of metallic ions (Mathews & Bekeny, 1979; Whitehead, 1961). Their development requires the convergence of ion flux which is realized by the vertical shear of horizontal neutral winds in a presence of an inclined magnetic field (Axford, 1963; Whitehead, 1961). Over the Brazilian sector, Resende et al. (2017a, 2017b) used the MIRE model (MIRE, Portuguese acronym for E Region Ionospheric Model) and observational data to show that the main contribution in forming these Es is the tidal winds shear mechanism. Recently, Resende et al. (2021) analyzed a set of 20 magnetic storms from 2015 to 2018 in different Brazilian regions, to observe the physical mechanisms in the Es layer formation. The authors used data from Boa Vista (BV, 2.8°N, 60.7°W, dip ~18°), São Luís (SLZ, 2.3°S, 44.2°W, dip ~8°), and CP (dip ~35°). They show that the Es layer in BV and SLZ can be affected by the electric field during disturbed magnetic times, besides the winds. However, over CP, they concluded that Es layer dynamics are dominated by the wind shear mechanism only. Therefore, tidal wind variability can directly affect the Es occurrence rate at the low/middle latitudes.

Thus, in the present work, we have analyzed the mesospheric diurnal and semidiurnal tides variability from April 1999 to December 2019 over CP and its possible relation with solar activity. Hence, we use a long data series, more than 16 effective years, to investigate the correlation of the SAO in the diurnal and semidiurnal tides with the 11-year solar cycle. The results show the evident anticorrelation between solar activity and tides, also reflected in the Es layer occurrence. Additionally, we present a possible mechanism involved in this coupling between geomagnetic activity and mesosphere-ionosphere. Thus, in the following sections, we will describe the equipment and the methodology employed in the data analysis in Section 3, we will show the results. Finally, we will present a scientific discussion and summary in Section 4.

2. Data Set and Methodology

An all-sky interferometric meteor radar inferred winds from 80 to 100 km of altitude at CP. This radar has a transmitting antenna that emits RF pulses at 35.24 MHz and receives the echoes on five receiving antennas. For each echo, the radial velocity of the meteor is determined, and the height, elevation, and azimuth are determined by the correlation between the signals from the various antennas and from the pulse delay (for more details, see Hocking & Thayaparan, 1997; Hocking et al., 2001). This radar allows resolutions of 1 hr in time and 2 km in altitude. Our analysis separated the echoes in 4 km height bins to avoid spurious wind variations due to low meteor counts and 1-hr time bins, building a monthly composite day for which the meridional and zonal winds were calculated and used to infer the annual, semi-annual and ter-annual components.

Wind data from April 1999 to December 2019 were analyzed, which had two main data gaps, August 2006 to September 2007 and from November 2008 to June 2012. Besides these two data interruptions, there are 196 individual months of good data. Data series encompass more than the 11-year solar cycle, bringing more consistency in the analysis. A least mean square fit was applied over each of the composite day wind data series to derive the mean wind and tidal components (for details, see Andrioli et al., 2009, Equation 1). The monthly means of tidal amplitudes are shown in Figure 1. We can clearly see the interannual variability in the diurnal and semidiurnal tidal amplitudes in different altitude range. Batista et al. (2004) analyzed meteor wind radar data at the same site. They found annual and semiannual variations in both diurnal and semidiurnal tidal amplitudes. Additionally, the vertical wavelength of the dominant mode in the diurnal tide was consistent with the $S_{1,1}$ (DW1) mode, first symmetric propagating Hough mode (Chapman & Lindzen, 1970), in good agreement with the GSWM model (Global Scale Wave Model, see Hagan et al., 1999 and Hagan & Forbes, 2002, 2003). Guharay et al. (2015) studied the variability in the diurnal tidal amplitudes and show a clear seasonal pattern with largest amplitude in fall equinox.

In sequence, we carried out a Lomb-Scargle spectral analysis, using the IDL code “scargle.pro” (from <http://astro.uni-tuebingen.de/software/idl/aitlib/timing/scargle.html>, for details see Scargle, 1982) to identify the main periodicities in the amplitudes of the diurnal and semidiurnal tides throughout the 16.5 years of data. In Figure 2 we can see the spectral power of the periodogram for the (a) zonal and (b) meridional diurnal tide, (c) zonal and (d)

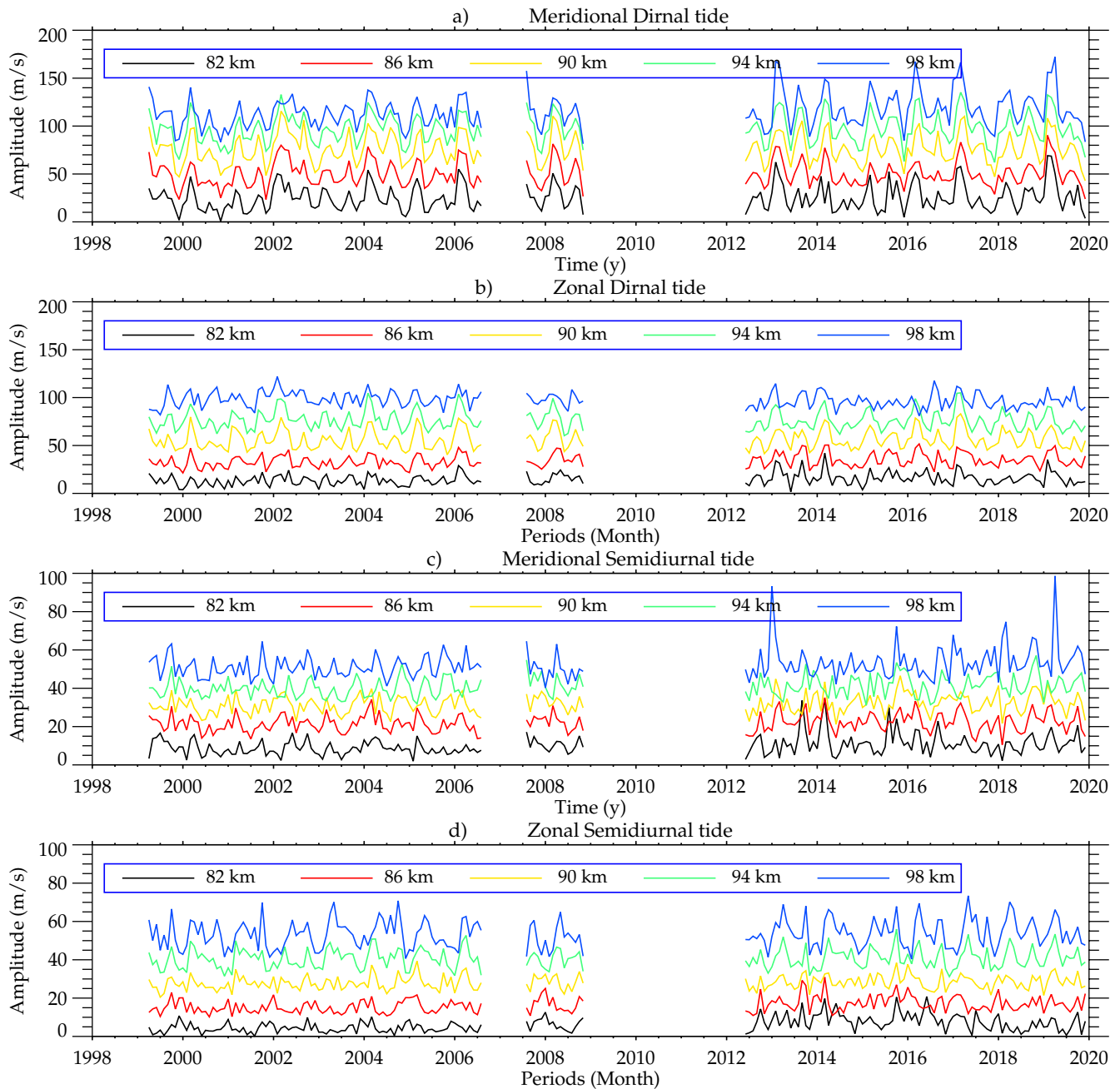


Figure 1. Monthly means tidal amplitudes observed at Cachoeira Paulista in 5 altitude ranges. Panel (a) meridional and (b) zonal diurnal tide; (c) meridional and (d) zonal semi-diurnal tide, from April 1999 to December 2019. Offsets plotted between successive 4 km altitudes are 20 m/s for the diurnal and 10 m/s for semi-diurnal tides.

meridional semi-diurnal tide at 5 altitude bins. Clear 6 (SAO) and 12 (Annual) months periodicities are evident in both diurnal and semi-diurnal tides in their zonal and meridional components. The power of SAO is stronger than annual periodicity for all components except for meridional semi-diurnal tide, where both seem alike. In addition, it is possible to observe some altitude variability. In fact, SAO is stronger around 90–94 km than other heights for all components. Note that the QBO, around 24-month period, does not reach the 95% confidence level at any altitude for all diurnal and semi-diurnal tide. The 11-year oscillation is not seen in this analysis since the Nyquist frequency for that is not reached.

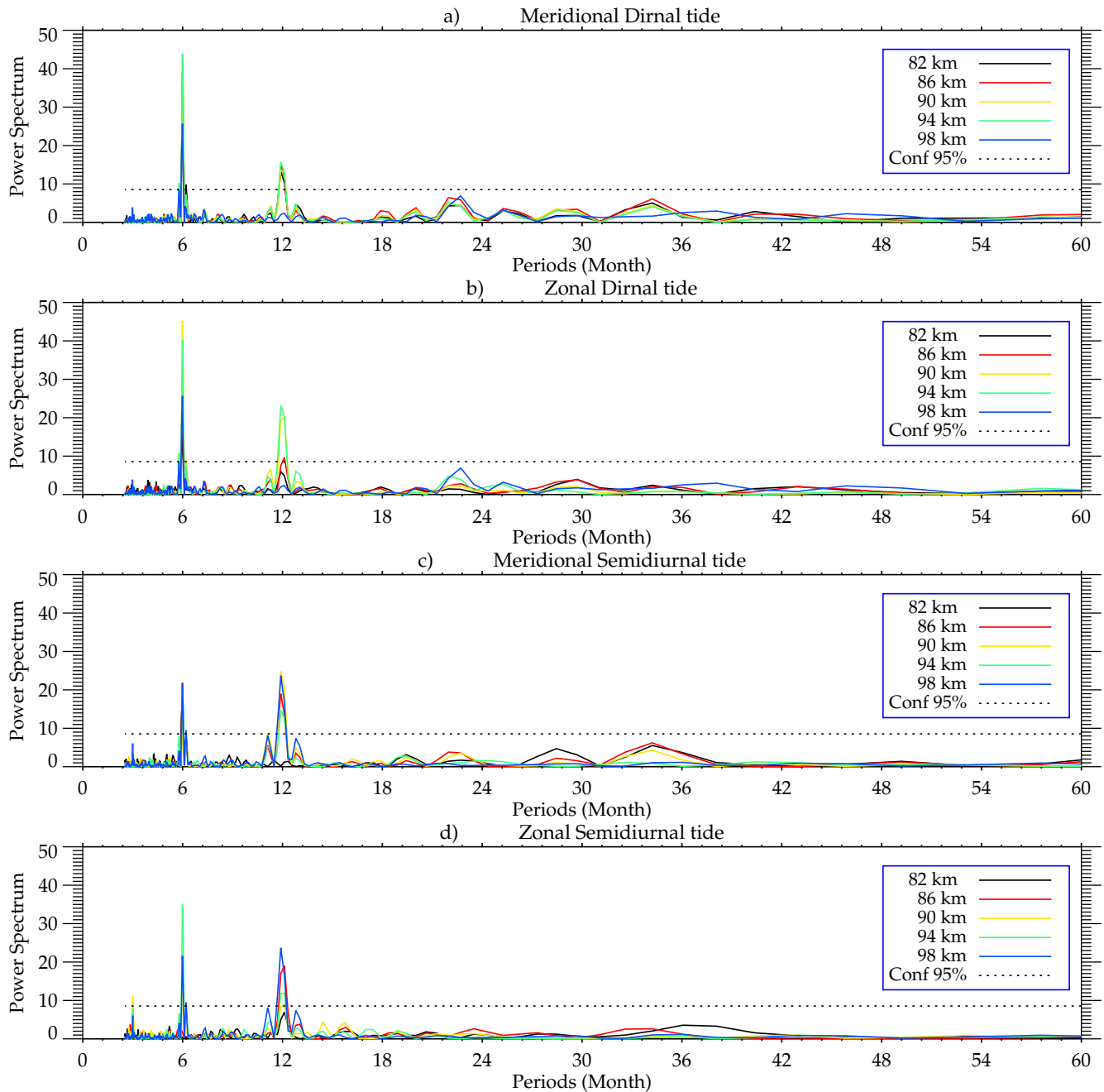


Figure 2. Lomb-Scargle Periodogram showing the Spectral Power for (a) zonal and (b) meridional diurnal tide, (c) zonal and (d) meridional semidiurnal tide, from April 1999 to December 2019 in different altitudes from 82 to 98 km. Dashed lines show the 95% significance levels.

Figure 3 shows the monthly averages of solar 10.7 cm flux for the same time of meteor radar data were observed. We can see clearly the 11-year solar cycle activity present in the solar flux. Furthermore, note that our analysis includes two regions of solar maximum and solar minimum activities conditions which give more credibility to the present study.

Afterward, we correlated the tidal amplitudes with the F10.7 cm solar flux by linear regression and obtained the correlation coefficient (R). Figure 4 shows the height distribution of R for diurnal (upper panels), and semidiurnal (bottom panels). Notice that both components show weak or no correlation with the 11-year solar cycle. The vertical blue dotted lines indicate 95% confidence applying the Student's t -test with 120 degrees of freedom.

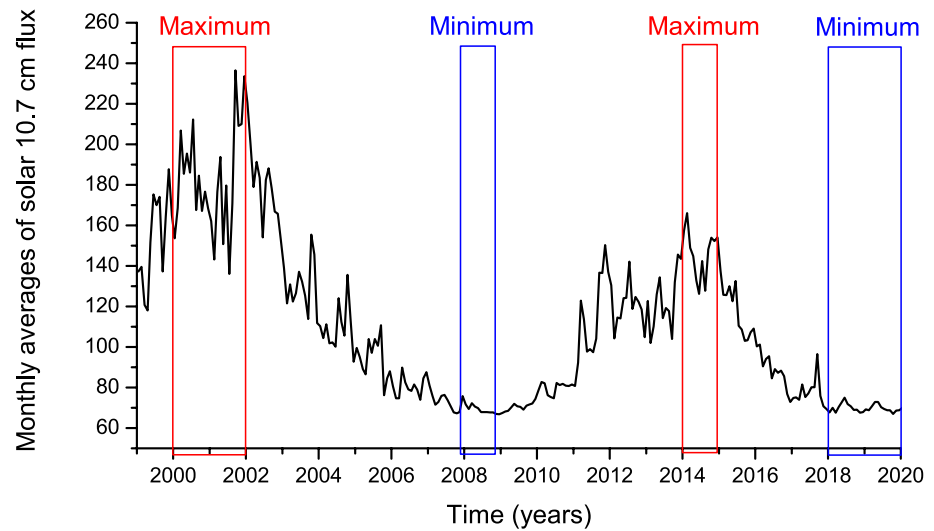


Figure 3. Monthly averages of solar 10.7 cm flux from January 1999 to December 2019. The boxes indicate periods representative of maximum and minimum solar activity used in the analysis showed in Figure 6. Data source: <http://www.spaceweather.gc.ca/solarflux/sx-en.php>.

Thus, we can see only a weak or not significant correlation when analyzing the tidal amplitude and solar cycle directly. Because atmospheric tides are global oscillations, any effect due to solar radiation would be more effective during the equinoxes when the Earth hemispheres are equally illuminated. Therefore, it is plausible to think that these effects would be more noticeable in the tidal SAO.

In this sense, we computed the 12- and 6-months amplitudes by using a least mean square harmonic fit, similar to that used in the previous tidal analysis. However, in this case, we used a 12-month window and shifted one month at a time. Subsequently, we correlated these results with a 12-point running mean of the monthly F10.7 Solar Flux. It is important to evaluate the confidence levels for the correlation coefficients. Nevertheless, we need to infer the correct degrees of freedom available in the sample. Fleenor et al. (2008) showed that one degree of freedom is consumed by each data point that is used in the moving average calculation and proposed an equation to determine the percentage of remaining degrees of freedom by:

$$Rdf = 100(1 - (Udf/Odf)) \quad (1)$$

where Rdf is the remaining percentage of degrees of freedom, Udf is the used degree of freedom in the moving window, and Odf is the original degree of freedom of the sample.

Assuming that our analysis is equivalent to a moving average, we have used this equation to infer the degree of freedom pertinent to our analysis and the respective confidence level for each correlation coefficient inferred by applying the Student's *t*-test. For the annual and semi-annual fit analysis, we have used a window of 12 points (12 months). According to Fleenor et al.'s work, Rdf is 93% of the original 194 df. These give us 180 degrees of freedom for the semi-annual/annual analysis. Hence, we decided to keep applying the test at 120 df for all analyses presented in this work. In this case, a narrower confidence level leaves equate to more reliable correlation coefficients. Additionally, we used the data obtained from the Digisonde installed at CP to evaluate the sporadic E (Es) layer occurrences. This equipment is a radar that transmits radio waves continuously into the ionosphere ranging from 1 to 30 MHz (Reinisch et al., 2009). We manually checked the data every 10 min using the SAO-Explorer software since significant discrepancies can be found between the automatically scaled and the correct values over the Brazilian stations (Resende et al., 2020). The ionosondes provide the ionospheric profile in graphs of frequency versus virtual height, from which it is possible to obtain the desired parameters.

The physical processes related to the correlation between solar activity and the tidal amplitudes are discussed here, considering the two main solar wind structures: interplanetary coronal mass ejections (ICMEs) and High-Speed solar wind Streams (HSSs). Thereby, we use the solar wind parameters at the L1 Lagrangian point obtained from the Magnetic Field Experiment (MAG) and the Solar Wind Electron, Proton, and Alpha Monitor (SWEPAM)

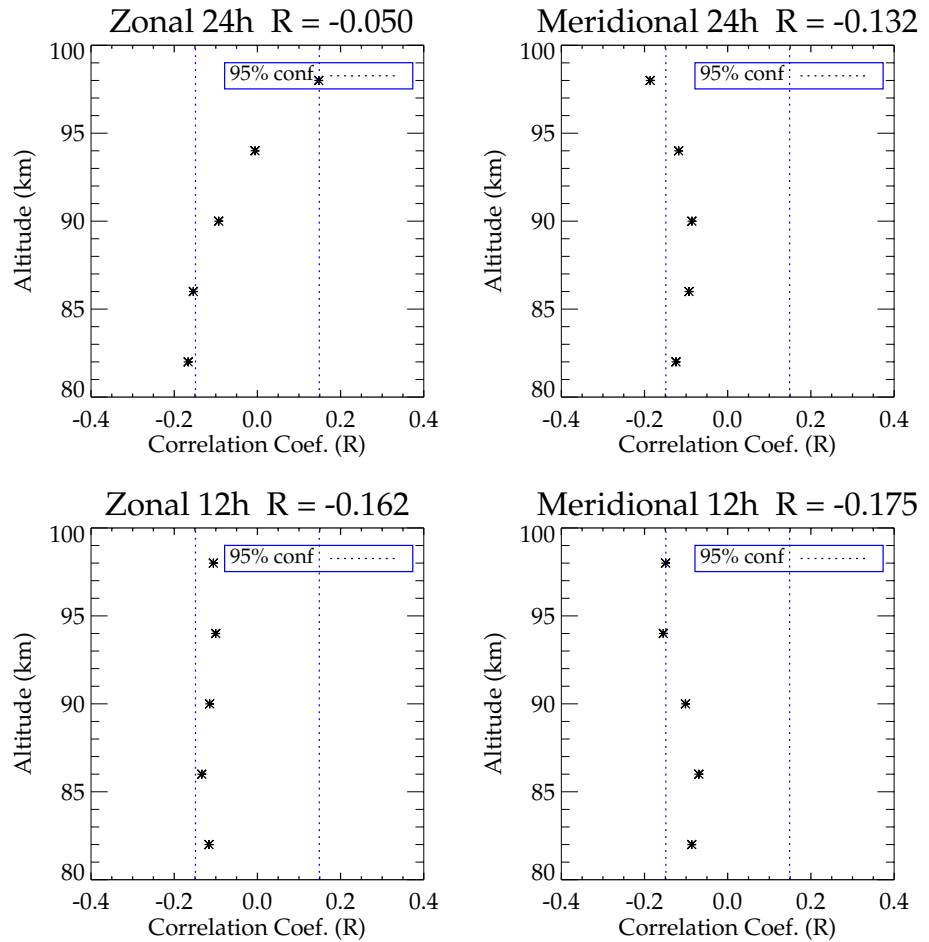


Figure 4. Correlation coefficients between tides and Solar Flux (F10.7 cm): diurnal (upper panels) and semidiurnal (bottom panels). Blue dotted vertical lines indicate 95% confidence applying the t-Student's t -test with 120 degrees of freedom. The written values at the top represent the correlation coefficient between height vector averaged tide amplitude and F10.7 cm Solar Flux.

instruments onboard the Advanced Composition Explorer (ACE) spacecraft (Stone et al., 1998). The Auroral Electrojet (AE) index with a 1-min time cadence and the Symmetric disturbance index (SYM-H) are used to discuss the role of the substorms/storms during the energy's deposit in the magnetosphere.

DONKI repository (Database Of Notifications, Knowledge, Information) is used to confirm the presence of the HSSs. In contrast, the catalog compiled by Cane and Richardson (2003) and Richardson and Cane (2010) is used to confirm the presence of the CMEs.

The high and low solar wind activity conditions are analyzed applying superposed epoch analysis (SEA). The scientific community widely uses this technique to identify whether a given type of event may have influenced a physical process that is either intrinsically random or their measurements are governed by random noise (Jamison & Regal, 1979).

3. Results

Figure 5 shows the correlation coefficients between 12-points moving averaged F10.7 Solar Flux and the amplitude of SAO in diurnal and semidiurnal tidal amplitudes for the zonal and the meridional components. A significant relationship between them is observed at almost all altitudes. In addition, we can observe that in both the diurnal and semidiurnal tides, the SAO amplitude is in anti-phase with the solar cycle. Note that all values of R reached the confidence level of 99% at 94 km. As shown by Batista et al. (2004) the diurnal tide reaches its

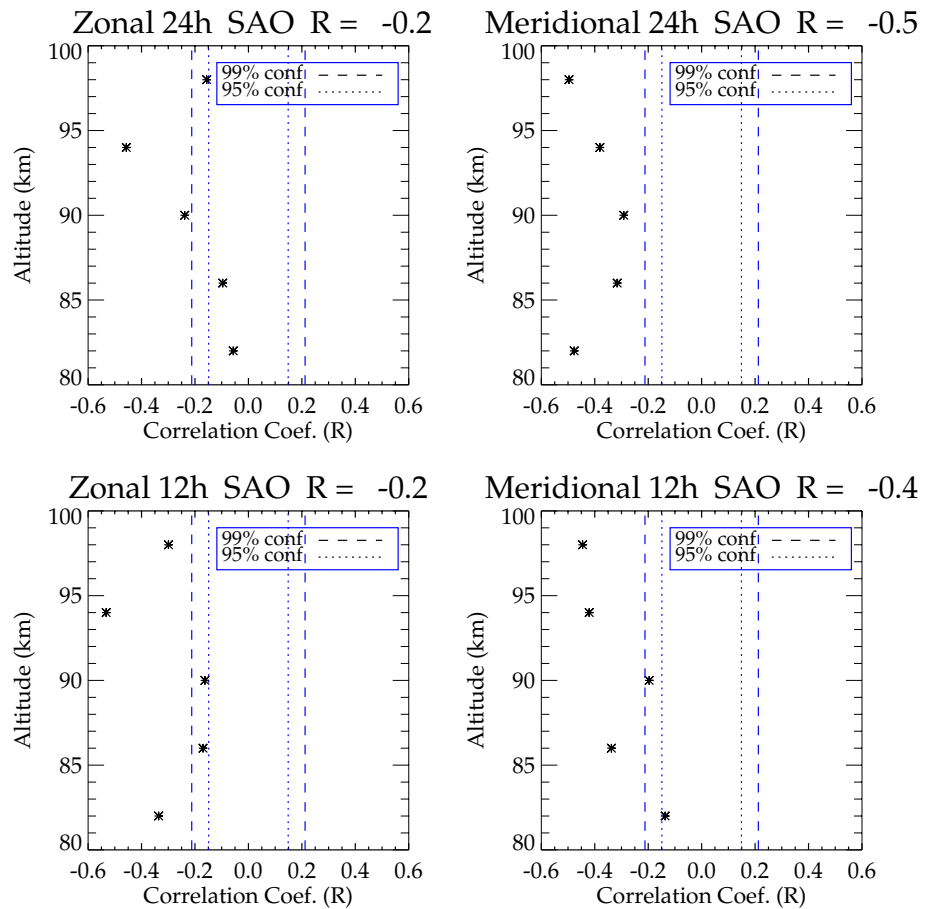


Figure 5. Correlation coefficients between semi-annual oscillation (SAO) and 12-points moving average in Solar Flux (F10.7 cm): diurnal (upper panels) and semidiurnal (bottom panels). The blue dotted (dashed) vertical lines indicate 95% (99%) confidence applying the Student's t -test with 120 degrees of freedom. The written values at the top represent the correlation coefficient between height vector averaged tide amplitude and F10.7 cm Solar Flux.

maximum amplitude at CP around this altitude. We can also observe the height variability of the correlation coefficients showing highest significance around 94 km for most of the components, which will be discussed ahead.

In order to investigate this anticorrelation and whether or not the amplitudes of tides are increased in the solar minimum we performed the following comparison. Diurnal and semidiurnal tide amplitudes observed in the years representative of minimum solar activity (from December 2007 to November 2008 and 2018 to 2019) were averaged into their corresponding month and height. The same was performed for those observed in the years representative of maximum solar activity (2000 to 2001 and 2014). These time periods are indicated by boxes in Figure 3 to emphasize the solar F 10.7 cm condition during the corresponding analysis. A total of 72 months were used, 36 during the minimum and 36 during the maximum solar activity. Subsequently, we divided these averaged values obtained in the minimum by those in maximum solar activity. The histograms showing these rates distributions are shown in Figure 6, left panels corresponds to diurnal tide and right ones to semidiurnal tidal ratios. We can observe in both panels that most of the values are greater than 1. It means that the tidal amplitudes are generally stronger during solar minimum than in solar maximum period. The larger differences between solar minimum and solar maximum amplitudes are in meridional component, where the diurnal tide amplitude is on average about 30% and semidiurnal is about 28% stronger during solar minimum against ~14% and 20% in the zonal component, respectively. In addition, note height variation of this rates, showing higher rates in the lower altitudes in diurnal tides. In the case of semidiurnal tide, the larger differences are observed around and above 86 km. These results reinforce the anti-correlation between solar activity and tidal amplitudes in the MLT region.

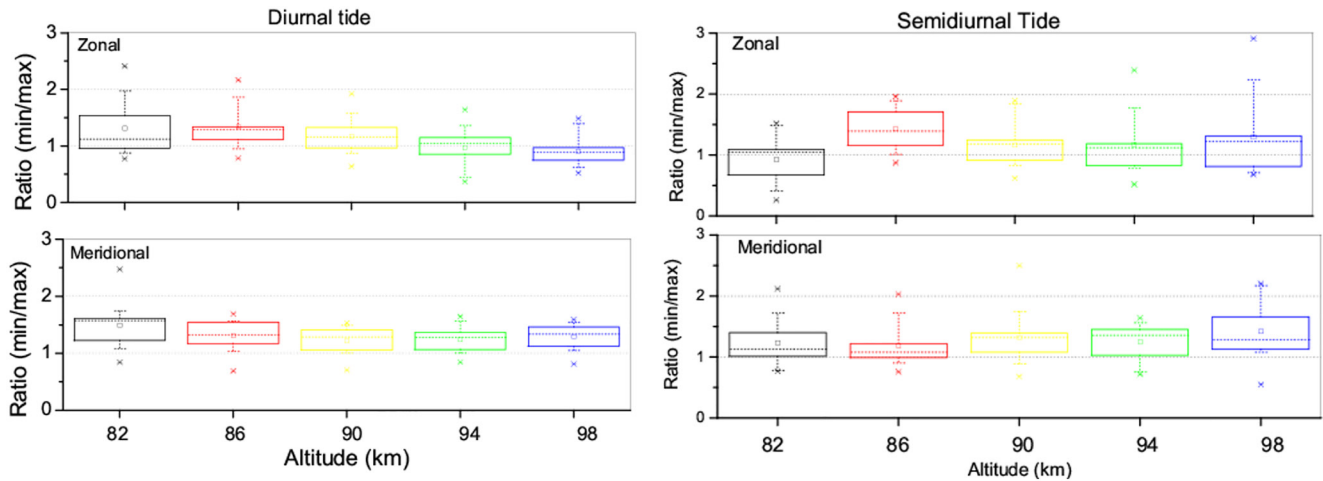


Figure 6. Histograms showing the ratios between monthly averaged tidal amplitudes during solar minimum and solar maximum activity. The upper panel represents the zonal component, and the bottom is the meridional one. The box is determined by the 25th and 75th percentiles. The whiskers are determined by the 5th and 95th percentiles. Cross points indicate minimum and maximum values, mean values is indicated by the square and the median is represented by dashed line inside the box.

One consequence of the tidal wind variability can be observed in the Es layer formation in CP. Figure 6 shows the occurrence of Es layers during 2015 (representative of a solar maximum in blue bars) and 2018 (representative of solar minimum in orange bars). Specifically, each panel in this figure corresponds to a composite of 3 months: (a) Summer (December, January, and February), (b) Autumn (March, April, and May), (c) Winter (June, July, and August) and (d) Spring (September, October, and November). The main feature in the Es layer behavior is the daily and seasonal variation in both scenarios: minimum and maximum solar activity. These variabilities are due to the seasonal meteor rate, the daily variation in the E region ionization, and the seasonal tidal wind variation, as shown in Resende et al. (2017a). However, we show a clear anti-phase difference in the Es layer occurrences concerning the solar cycle for the first time in the Brazilian sector. Notice that the Es layer rate is larger during solar minimum than the solar maximum at all hourly seasonal distribution. Therefore, this result supported our analysis showed before, in which there is a solar cycle influence over the winds in these heights.

4. Discussion and Summary

We have used meteor radar wind measurements made at Cachoeira Paulista, Brazil, over 21 years to evidence the solar activity influence in the amplitudes of the semidiurnal and diurnal tides in the MLT region. Correlating the tidal fields with the solar flux lower solar influences were found which agrees with several previous works (e.g., Jacobi, 1998; Oberheide et al., 2009). Notwithstanding, Jacobi (1998) showed that the spring and summer zonal prevailing wind was negatively dependent on the solar activity, meaning the westerly winds were weaker during solar maximum. And the studies done by Oberheide and collaborators showed negative correlation between diurnal tide and solar cycle above 120 km and increasing with altitude. Although the lower correlations presented in direct analysis, diurnal and semidiurnal tides showed a significant negative correlation with solar cycle activity highlighted in the semiannual variation. These anticorrelations of tidal activity and solar cycle have also been showed by several works in different latitudes and also in other seasons (Bremer et al., 1997; Greisiger et al., 1987; Guharay et al., 2019; Iimura et al., 2010; Jacobi et al., 1997; Namboothiri et al., 1993; Sprenger & Schminder, 1969; Sridharan et al., 2010). Sridharan et al. (2010), using data from MF radar at Tirunelveli (8.7°N), have found negative Solar Cycle response during all the months only in meridional diurnal tide winds. Singh and Gurubaran (2017) analyzed tidal variability at same site and compared with temperature and wind from SABER. Their results showed an interesting result about a possible solar cycle influence on the diurnal tide, a feature which is more prominently seen in radar observations than the satellite data, though restricted to a certain epoch of the solar cycle. The differences in radar results and satellite data as well as the solar cycle dependence presented only in meridional component show how complex can be the interaction of solar activity and tidal amplitudes.

Guharay et al. (2019) investigated the solar cycle dependence of the tides in the low latitude MLT using meteor radar. Although their analysis did not show any significant relationship between the long-term variation of the tides and solar activity, the individual seasonal profiles reveal a negative correlation of diurnal and semidiurnal tides in the equinoxes. Correlations between the semiannual variations of the diurnal and semidiurnal tides with solar activity have not been reported previously. Meanwhile, the results presented by Guharay et al. (2019) can be interpreted as agreeing to the present since their analysis consider the seasonality of the tides, which is another way to evaluate SAO. As mentioned above, Earth hemispheres are equally illuminated during equinoxes, evidencing any effect due to solar activity in the tidal amplitudes. Hence their results are in good agreement with this work. Emmert and Picone (2010) performed a detailed climatological analysis of daily globally averaged density data in Thermospheric altitudes (250, 400 and 550 km). They found that amplitudes of the annual and semiannual harmonics increase with height and with F10.7 solar flux. Moreover, Jones et al. (2017) and (2018) demonstrated that the global average thermosphere and ionosphere SAO in mass and electron densities are strongly influenced by tidal dissipation in the MLT region. The solar cycle variability of the global average thermosphere and ionosphere SAO (as shown in Emmert and Picone [2010], Figure 5) is positively correlated. However, it is still not explained what causes this solar cycle variation in the upper thermosphere and ionosphere global average SAO. As shown here, tidal amplitudes at CP decrease with increasing F10.7. Perhaps, decreased tidal mixing during solar maximum in the MLT region, could lead to increased global average SAO amplitudes during solar maximum in the upper thermosphere and ionosphere. This is speculative and can lead to some future work explaining this coupling.

In addition, Emmert and Picone (2010) reported that the correlation between SAO and F10.7 index is not strong, and the interannual variability of the amplitudes is comparable to their increase from solar minimum to solar maximum. Although the altitudes of the present study are much lower than previous work, we use their last result as a good argument to rate the amplitudes in solar minimum to solar maximum. Figure 6 presented the ratio between amplitude of diurnal and semidiurnal tides observed in the solar minimum and solar maximum period, and it is noted that indeed the tidal amplitudes are stronger during solar minimum than the solar maximum. This analysis made evident the strongest diurnal (semidiurnal) amplitudes, meridional $\sim 30\%$ ($\sim 28\%$), and zonal $\sim 14\%$ ($\sim 20\%$) on average, during solar minimum, reinforcing their anticorrelation with solar activity. This variation in the tidal amplitudes is reflected in the Es layer development, as shown in Figure 7, in which the occurrence of this layer is much higher during solar minimum than in solar maximum. Es layer occurrences in Cachoeira Paulista have been studied for decades (e.g., Abdu & Batista, 1977; Batista & Abdu, 1977) but this is the first time the difference in Es occurrences between minimum and maximum solar cycle activity is presented. In a more recent work, Resende et al. (2021) showed that over this site, the Es layer dynamics are dominated by the wind shear mechanism, not being influenced by the electric field. Hence, the anticorrelation seen in the frequency of the Es layer is probably a consequence of the impact of solar activity in tidal winds. The relation between solar activity and Es occurrences was also investigated by other authors in different latitudes (e.g., Niu et al., 2019; Pezzopane et al., 2015; Zhang et al., 2015; Zuo & Wan, 2002). Niu et al. (2019) found both positive and negative correlations between sporadic E intensity and solar activity that depended on magnetic latitude. Pezzopane et al. (2015) have found both positive correlations between the F10.7 solar index and foEs as well as between F10.7 and fbEs, for midlatitude. Furthermore, Zhang et al. (2015) studied the influence of solar and geomagnetic activity on Es layers over low, mid and high latitude stations. Their results showed different solar activity correlation depending on latitude station. At low and mid latitude, the correlation coefficients of Es layer with solar activity are positive in daytime and negative in nighttime. The coefficients are positive for low intensive layers and negative for high intensive layers in daytime, and they are all negative in nighttime. The present results do not show any difference between day to night correlations. Although the influences of solar cycle on Es layer deserves more investigations our results show evidences that the stronger tidal amplitudes in the minimum solar cycle are the main responsible for the anticorrelation between solar cycle and Es occurrences at Cachoeira Paulista.

Several authors tried to explain the anticorrelation between tidal amplitudes and 11-year solar cycle. Baumgaertner et al. (2005) suggested amplitude variations of the planetary wave number 1 as possible explanation for their observation in the semidiurnal tide. Their explanation is based on the assumptions regarding the specific semidiurnal tide modes observed at Scott Base. However, the negative correlation of the semidiurnal tide has also been observed at low and middle latitudes where the semidiurnal tide is dominated by the migrating mode (Forbes, 1982a, 1982b; Hagan & Forbes, 2003) and the explanation by Baumgaertner et al. (2005) cannot be applied at these latitudes. Another possibility for the explanation of a decrease in the tidal amplitudes during solar

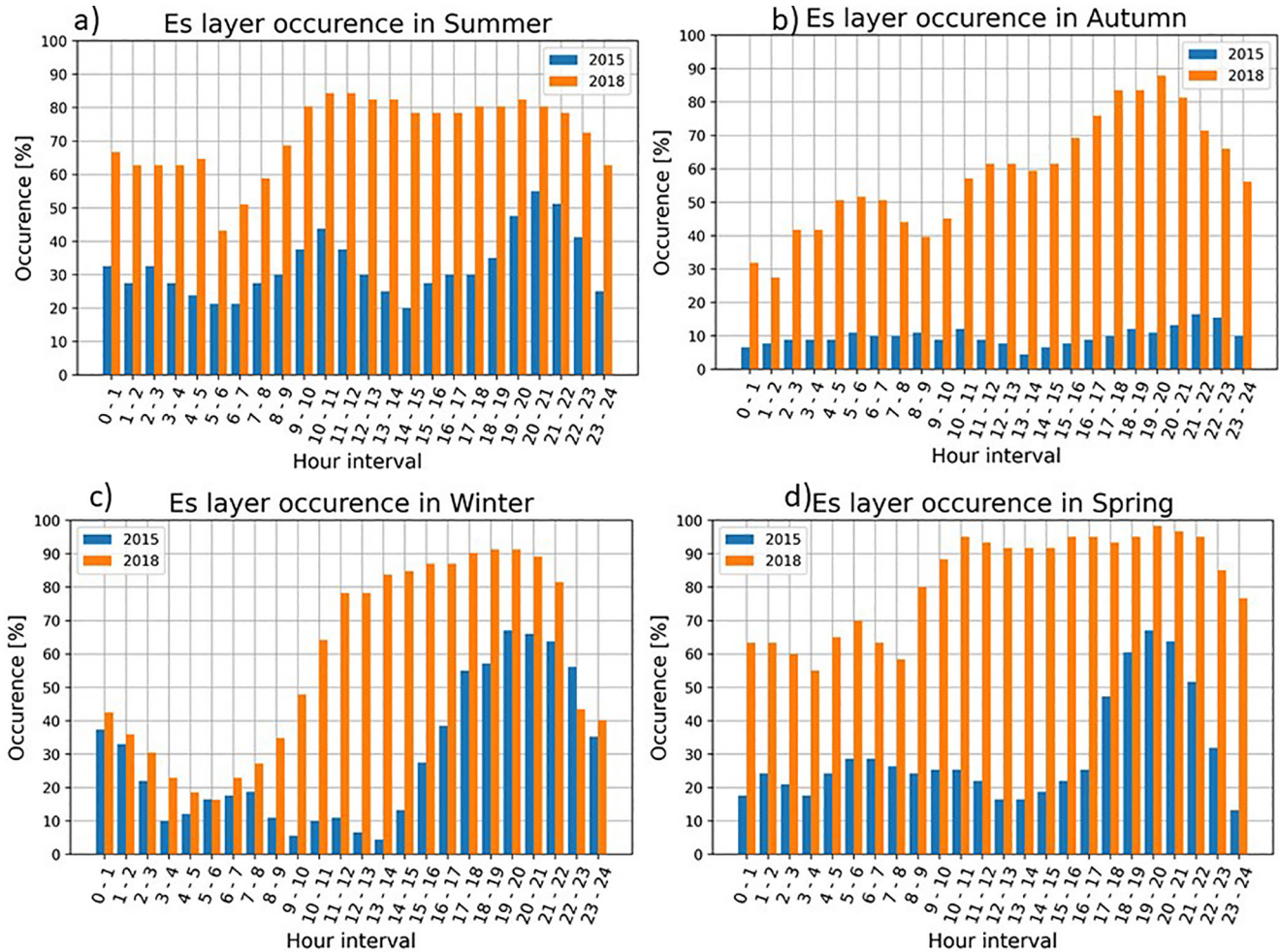


Figure 7. Hourly distributions of Es layer occurrence during 2015 representative of solar maximum (blue bars) and 2018 representative of solar minimum (orange bars) observed in Cachoeira Paulista. Each panel corresponds to a composite of 3 months: (a) Summer (December, January, and February), (b) Autumn (March, April, and May), (c) Winter (June, July, and August) and (d) Spring (September, October, and November).

maxima is a slower growth of tidal amplitudes with altitude due to an increase in the mean densities at higher altitudes. This is because migrating tides are excited by ultraviolet (UV) light absorption by O_3 in the stratosphere and propagates upward and grows in amplitude as neutral atmospheric density decreases due to conservation of mass and energy (Chapman & Lindzen, 1970; Forbes & Garrett, 1979; Holton, 1973). Higher stratospheric temperatures during solar maximum are expected to lead to somewhat higher mean densities at higher altitudes (Schmidt et al., 2006). Besides all those efforts, it is not clear at this stage which of the various competing influences most strongly impacts tidal amplitudes at this time.

Yi, Reid, Xue, Younger, Spargo, et al. (2017) reported for the first time the mesospheric density responses due to Solar Wind High-Speed Stream (HSS) in Antarctica. They observed periodic structures in the mesospheric densities at 90 km, similar to the periodic structures in HSS. Their findings showed evidence of a coupling mechanism between the mesosphere and magnetosphere-ionosphere-thermosphere (MIT) system, which is still not well understood. Furthermore, Tsurutani et al. (2019) commented that article suggesting possible physical mechanisms for those observations. They suggested that low-energy electrons precipitate into the mesosphere during HSS events, depositing most of their energy from ~ 85 to ~ 95 km altitude range. They cited the work by Thorne (1980) which showed that the precipitation of ~ 10 - to 100 -keV substorm electrons lead to the ionization and dissociation of nitrogen (N_2) molecules with the ultimate formation of nitric oxide (NO). The formation of NO will radiate infrared and also catalytically lead to the destruction of ozone (O_3) and therefore cause a lack of solar ultraviolet absorption in the region. This will lead to effective mesospheric cooling and modulation of local

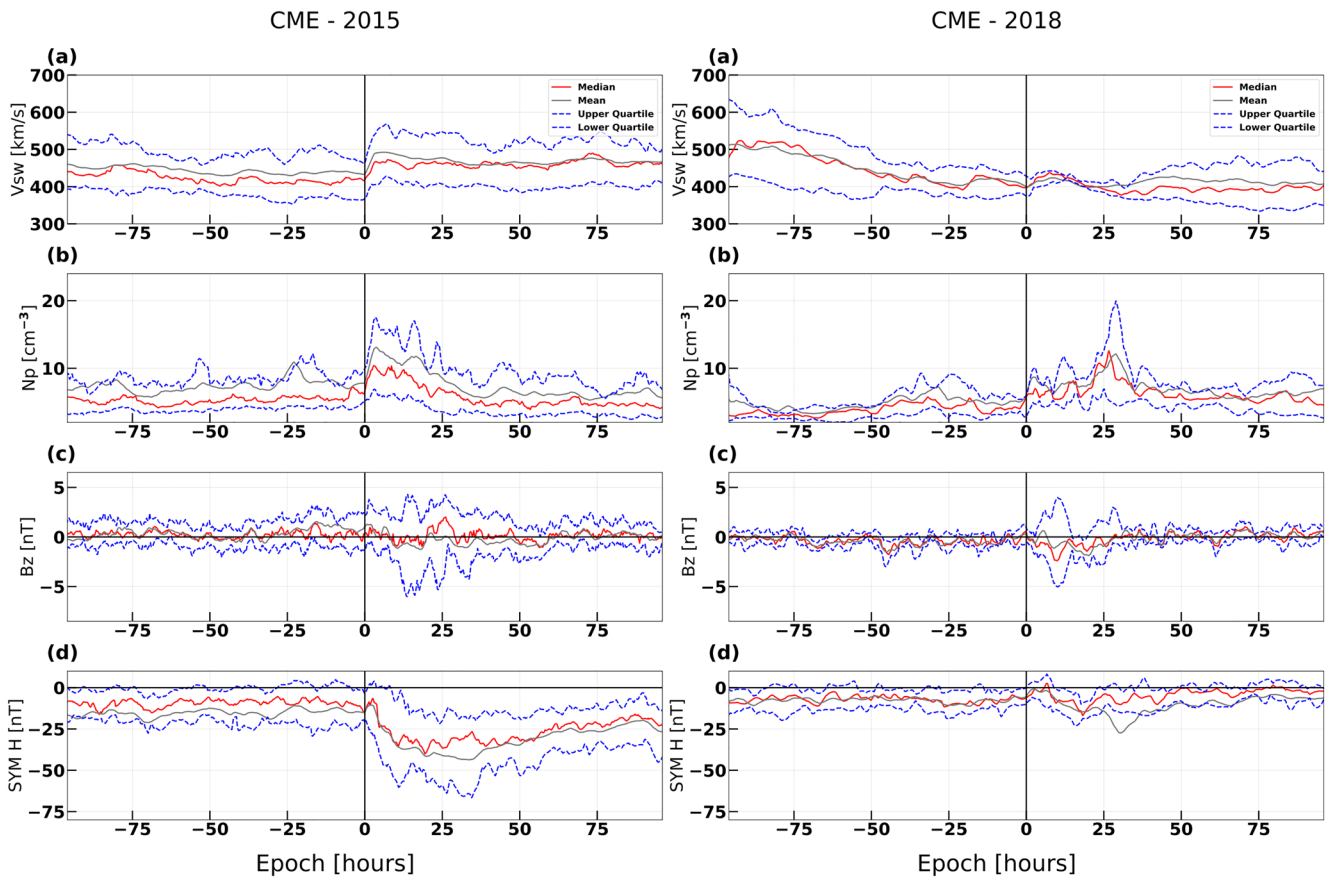


Figure 8. Superposed Epoch analysis for the solar wind parameters under the influences of the Interplanetary Coronal Mass Ejections (ICMEs) during the solar maximum (2015) and minimum (2018) of the solar cycle 24. The solid red line corresponds to the median, the gray line represents the mean, while the dashed blue ones are the upper and lower quartiles. From top to bottom: solar wind speed, proton density, Interplanetary Magnetic Field (IMF) Bz, and SYM-H index.

winds and neutral densities. Besides the work presented by Yi, Reid, Xue, Younger, Murphy, et al. (2017) and Yi, Reid, Xue, Younger, Spargo, et al. (2017) other authors have studied mesosphere-ionosphere-thermosphere responses during HSS events. Chang et al. (2009) and Mukhtarov and Pancheva (2012) based on the SABER/TIMED temperature measurements and considering different periods demonstrated the forcing of the zonally symmetric planetary waves with period of the solar wind HSS.

The above works show indications of the coupling between HSS and mesosphere-ionosphere-thermosphere during declining phase of solar cycle. Here, we analyze the interplanetary medium conditions under the influence of the ICMEs and HSSs during the solar maximum and minimum of the solar cycle 24. Figures 8 and 9 show the superposed epoch analysis of the solar wind parameters measured at the L1 Lagrangian point and the SYM-H and AE indices. SYM-H index is used to discuss the storms' intensity during the ICMEs, while the AE index is used to discuss the substorms' intensity during the HSSs. The zero epoch of the time series for the epoch overlap analysis. This work uses the time of the solar wind structures' arrival at the Earth's magnetosphere, obtained in the Donki and Richardson & Cane lists, to define the zero epoch.

Figure 8 shows the epoch analysis of the solar wind parameters under the influence of the ICMEs during the solar maximum (2015 – left panels) and solar minimum (2018 – right panels). The median values of the solar wind parameters and SYM-H index after the zero epoch, specifically in the first 12 hr, are considerably high during the solar maximum in comparison with the solar minimum. The SYM-H index reaches -40 nT during the solar maximum (left panel d), while it reaches -20 nT during the solar minimum (right panel d). The solar wind velocity and proton density during the solar maximum (left panel a–b) reach values above 450 km/s and 10 protons/cm³, respectively. In comparison, during the solar minimum (right panel a–b), it reaches values below 450 km/s and 10 protons/cm³, respectively.

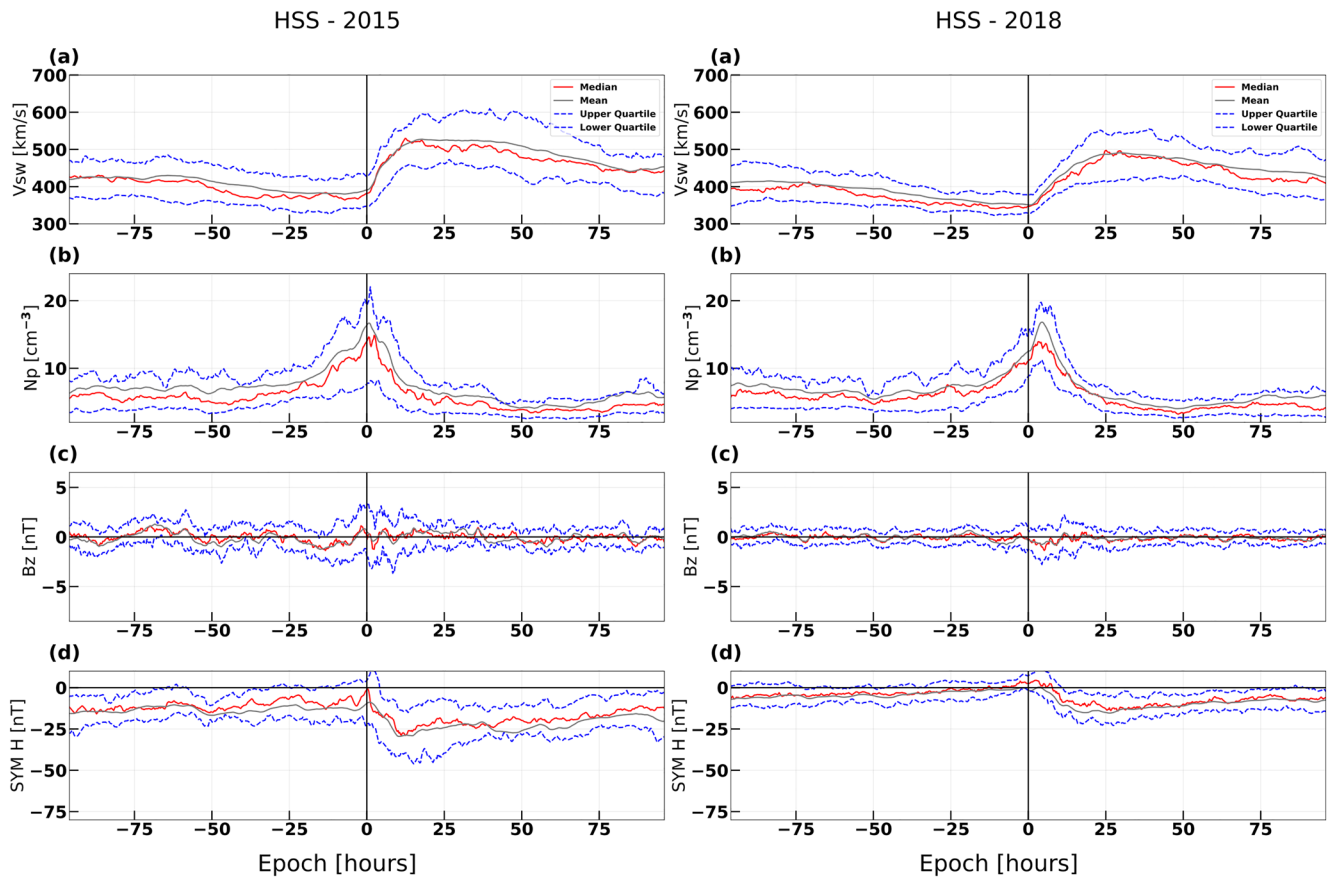


Figure 9. Superposed Epoch analysis for the solar wind parameters under the influences of the High-Speed Solar Wind Streams (HSSs) during the solar maximum (2015) and minimum (2018) of the solar cycle 24. The solid red line corresponds to the median, the gray line represents the mean, while the dashed blue ones are the upper and lower quartiles. From top to bottom: solar wind speed, proton density, Interplanetary Magnetic Field (IMF) Bz, and Auroral Electrojet (AE) index.

The majority of strong storms are driven by ICMEs, with a short recovery phase, typically a couple of days (e.g., Echer et al., 2008; Tsurutani & Gonzalez, 1997). Consequently, the interplanetary medium conditions analyzed in Figure 7 can trigger the dynamic mechanisms to deposit energy into the magnetosphere (Ponomarev et al., 2006), which can be more efficient during the solar maximum than the solar minimum. The impact of these geomagnetic storms in the inner magnetosphere is widely discussed in the literature, such as observed through the outer radiation belt's electron flux variability (Da Silva, Shi, Alves, Sibeck, Souza, et al., 2021; Murphy et al., 2018; Turner et al., 2019). The rapid electron flux decreases generally are observed during the occurrence of the strong geomagnetic storms associated with the ICMEs (Da Silva, Shi, Alves, Sibeck, Souza, et al., 2021; Turner et al., 2019), and the electron particles precipitation to the atmosphere can also occur quickly.

Figure 9 shows the epoch analysis of the solar wind parameters under the influence of the HSSs during the solar maximum (2015–left panels) and minimum (2018–right panels). Although the median values of the solar wind parameters after the zero epoch, specifically in the first 50 hr, have been slightly high during the solar maximum in comparison with the solar minimum, it is essential to highlight that these HSSs compete with strong storms associated with ICMEs in 2015. It means that the dynamic mechanisms associated with HSSs may be masked or embedded into the ICMEs during the solar maximum.

The substorms driven by HSSs are persistent for a long duration, that is, from a few to ~10 days (Richardson et al., 2006; Tsurutani et al., 1995). Consequently, they may deposit more energy in the magnetosphere than the ICME-driven storms (Miyoshi & Kataoka, 2005; Turner et al., 2006), principally if compared with the ICMEs moderate and weak as occur in 2018. Although the AE index during the solar maximum (left panel d) presented values higher than during the solar minimum (right panel d), Da Silva et al. (2019), Da Silva, Shi, Alves, Sibeck, Marchezi, et al. (2021) shown that weak substorms (AE index <300 nT) are also efficient to inject the low-energy

Superposed Epoch analysis HSS events Occurred in 2018

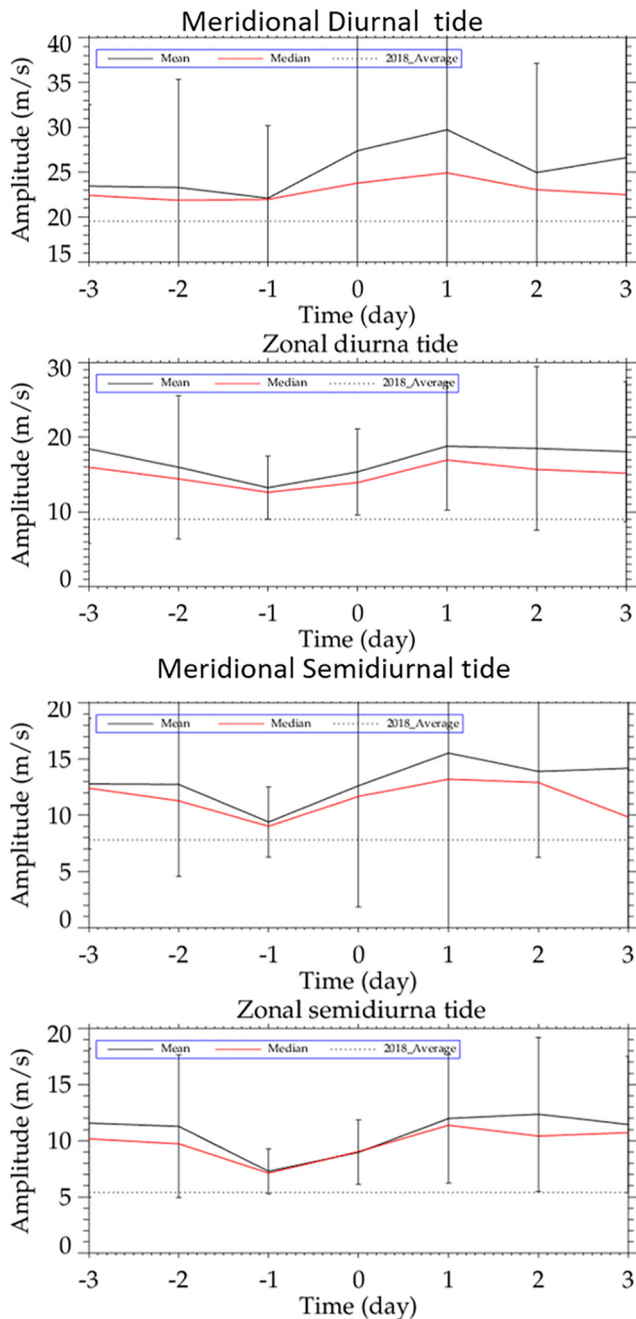


Figure 10. Superposed Epoch analysis for the height vector averaged meridional and zonal diurnal (upper panels) and semidiurnal (bottom panels) amplitudes under the influences of the High-Speed Solar Wind Streams (HSSs) during the solar minimum (2018). Zero Epoch is the day when the structures reach the Earth. Black dotted line is the total median, that means a median calculated for each component considering all data set. Black straight line is the mean and the error bars represent the its standard deviation; Red straight lines represent the median values.

electron flux in the outer radiation belt, to be accelerated. Consequently, the low-energy electron particle precipitation also occurs under the influences of the weak substorms and for a long duration.

The mesosphere density response to solar activity has been reported by several authors using satellite (Singh & Gurubaran, 2017) and by ground measurements (Stober et al., 2014; Yi, Reid, Xue, Younger, Murphy, et al., 2017). Stober et al. (2014) reported mesosphere density variation with the solar cycle using Canadian Meteor Orbit Radar data. They observed a variation of $2.4 \pm 0.7\%$ in the mesosphere density with solar cycle. Singh and Gurubaran (2017) presented a solar cycle dependence of the zonal mean densities observed in satellite data 87 km altitude. Their results revealed that the background neutral densities are larger during the solar maximum years and smaller during the solar minimum years which appears to be a plausible source for the observed solar cycle signature in the diurnal tide. Yi, Reid, Xue, Younger, Murphy, et al. (2017) reported an analysis of the neutral mesosphere density response to geomagnetic activity between 2016 and 2017. Their results showed a significant decrease in neutral residual mesospheric density as the geomagnetic activity enhances. Besides this anti-correlation between the geomagnetic activity and mesospheric density, they found a strengthening response with decreasing altitude. Additionally, they also reported a more substantial effect on the dayside density than the night-side density. The authors proposed that the energetic particles, present during HSS events, directly penetrate into the mesosphere from the Earth's radiation belts, causing a depletion of mesospheric O_3 (for e.g., Andersson et al., 2014; Fyter et al., 2015; Turunen et al., 2016). This would lead to the loss of radiative heating by O_3 absorption, leading to a temperature reduction and a decrease in mesospheric density. This suggestion, although speculative, is consistent with their results.

Among Yi, Reid, Xue, Younger, Murphy, et al. (2017) results, it is interesting to point out here the higher amplitudes presented in the mesospheric density structures during dayside than the nightside. This difference in atmospheric forcing from day to night can contribute to the 24 hr oscillation. Although this mechanism acts in the auroral regions, as global waves, atmospheric tides could be sensitive to this mechanism. The waves with a period within day harmonics, forced around the auroral region can expand, and their winds effects could reach lower latitudes. This could explain the larger meridional correlations coefficients as well as the larger meridional amplitude ratio than zonal. Another evidence in agreement with their results is the altitude dependence of the correlation coefficient, showing a higher correlation in the lower altitudes.

In order to reinforce our argument that particles precipitation during HSS events can affect tidal amplitudes in Cachoeira Paulista, a superposed epoch analysis of tidal amplitudes observed during events of HSS are presented in Figure 10. We first inferred the winds components using 4 km altitude and 1 hr time resolution, from 3 days before and 3 days after HSS event reaches the Earth. In the sequence, tidal amplitudes in 24 hr intervals were fitted and calculated their height vector averages using the range from 86 to 94 km, which is the region where the meteor counting is enough to minimize the error when using hourly wind calculation. These data were superposed and the zero epoch is considered the day when the HSS reached the Earth (using DONKI catalog). We can observe a slight increase in the tidal mean and median amplitudes in the day that the structure reach and in the following

days. This effect is observed in all diurnal and semidiurnal tidal amplitudes reinforcing this coupling between solar activity and tides.

Concerning Figure 10, note the large standard deviations of the mean shown in all four plots. These spread in the data can be caused by the difference in the energy deposition due to different amount of particle precipitating in each event. As shown in Figure 9 the HSS events are not uniform. Therefore, one important thing in this analysis is that even with the spread in the data, on average the amplitudes of tides show an increase after the HSS event occurrence.

This physical mechanism of tidal forcing in the auroral region and their propagation to lower latitudes should be evaluated deeply in observational and model results. Furthermore, we cannot neglect a possible local effect by particle precipitation in the South Atlantic Magnetic Anomaly (SAMA) region due to reduced magnetic field in this region. As presented by several works (e.g., Pinto & Gonzalez, 1989; Pinto et al., 1989; Gonzalez et al., 1987; Nishino et al., 2006; Da Silva et al., 2016) electron particle precipitation can occur in Cachoeira Paulista, especially under the influences of the geomagnetic storms and substorms. Therefore, the impact of solar activity in mesosphere due to SAMA is going to be investigated in a future work.

Finally, the present work showed evidence of an anticorrelation between the solar cycle and mesospheric tides. On average, the diurnal (semidiurnal) tide is enhanced around 30% (~28%) in meridional and 14% (~19%) in the zonal component during solar minimum activity. This effect was reflected in the Es layer occurrences. We explain observed results in terms of the HSS according to the solar cycle. Here, we suggested a possible physical mechanism that is tidal forcing due to difference in dayside to nightside particle precipitation during HSS events. Although more works are needed to evaluate this possibility, our analysis brings novel results that helps improving our understanding on coupling between solar wind activity with the mesosphere-ionosphere-thermosphere system.

Data Availability Statement

The all-sky meteor wind data can be found at: <https://doi.org/10.5281/zenodo.5510648>. The solar F10.7 flux: <http://www.spaceweather.gc.ca/solarflux/sx-en.php>. The Digisonde data from Cachoeira Paulista can be downloaded upon registration at the Embrace webpage from INPE Space Weather Program in the following link: <http://www2.inpe.br/climaespacial/portal/en/>. ACE: <http://www.srl.caltech.edu/ACE/ASC/DATA/browse-data/>. DONKI: <https://kauai.ccmc.gsfc.nasa.gov/DONKI/search/>. Richardson/Cane list: <http://www.srl.caltech.edu/ACE/ASC/DATA/level3/icmetable2.htm>. OMNIWeb: <https://omniweb.gsfc.nasa.gov/>.

References

- Abdu, M. A., & Batista, I. S. (1977). Sporadic-E layer phenomena in the Brazilian geomagnetic anomaly: Evidence for a regular particle ionization source. *Journal of Atmospheric and Solar-Terrestrial Physics*, 39, 723–731. [https://doi.org/10.1016/0021-9169\(77\)90059-9](https://doi.org/10.1016/0021-9169(77)90059-9)
- Andersson, M. E., Verronen, P. T., Rodger, C. J., Clilverd, M. A., & Wang, S. (2014). Longitudinal hotspots in the mesospheric OH variations due to energetic electron precipitation. *Atmospheric Chemistry and Physics*, 14(2), 1095–1105. <https://doi.org/10.5194/acp-14-1095-2014>
- Andrioli, V. F., Clemesha, B. R., Batista, P. P., & Schuch, N. J. (2009). Atmospheric tides and mean winds in the meteor region over Santa Maria (29.7°S; 53.8°W). *Journal of Atmospheric and Solar-Terrestrial Physics*, 71, 1864–1876. <https://doi.org/10.1016/j.jastp.2009.07.005>
- Araújo, L. R., Lima, L. M., Batista, P. P., & Jacobi, C. (2020). Behaviour of monthly tides from meteor radar winds at 22.7°S during declining phases of 23 and 24 solar cycles. *Journal of Atmospheric and Solar-Terrestrial Physics*, 205, 105298. <https://doi.org/10.1016/j.jastp.2020.105298>
- Axford, W. I. (1963). The formation and vertical movement of dense ionized layers in the ionosphere due to neutral wind shears. *Journal of Geophysical Research*, 68(3), 769–779. <https://doi.org/10.1029/JZ068i003p00769>
- Batista, I. S., & Abdu, M. A. (1977). Magnetic storm associated delayed sporadic-E enhancements in the Brazilian geomagnetic anomaly. *Journal of Geophysical Research*, 82, 4777–4783. <https://doi.org/10.1029/JA082i029p04777>
- Batista, P. P., Clemesha, B. R., Tokumoto, A. S., & Lima, L. M. (2004). Structure of the mean winds and tides in the meteor region over Cachoeira Paulista, Brazil (22.7°S; 45°W) and its comparison with models. *Journal of Atmospheric and Solar-Terrestrial Physics*, 66, 623–636. <https://doi.org/10.1016/j.jastp.2004.01.014>
- Baumgaertner, A. J. G., McDonald, A. J., Fraser, G. J., & Plank, G. E. (2005). Long-term observations of mean winds and tides in the upper mesosphere and lower thermosphere above Scott Base, Antarctica. *Journal of Atmospheric and Solar-Terrestrial Physics*, 67, 1480–1496. <https://doi.org/10.1016/j.jastp.2005.07.018>
- Bremer, J., Schindler, R., Greisiger, K. M., Hoffmann, P., Kürschner, D., & Singer, W. (1997). Solar cycle dependence and long term trends in the wind field of the mesosphere/lower thermosphere. *Journal of Atmospheric and Solar-Terrestrial Physics*, 59, 497–509. [https://doi.org/10.1016/S1364-6826\(96\)00032-6](https://doi.org/10.1016/S1364-6826(96)00032-6)
- Burrage, M. D., Hagan, M. E., Skinner, W. R., Wu, D. L., & Hays, P. B. (1995). Long-term variability in the solar diurnal tide observed by HRDI and simulated by the GSWM. *Geophysical Research Letters*, 22, 2641–2644. <https://doi.org/10.1029/95GL02635>
- Cane, H. V., & Richardson, I. G. (2003). Interplanetary coronal mass ejections in the near-Earth solar wind during 1996–2002. *Journal of Geophysical Research*, 108(A4), 1156. <https://doi.org/10.1029/2002JA009817>

Acknowledgments

V. F. Andrioli would like to thank the China-Brazil Joint Laboratory for Space Weather (CBJLSW), National Space Science Center (NSSC), Chinese Academy of Sciences (CAS) for supporting her postdoctoral fellowship. We also thank to the Brazilian National Council for Scientific and Technological Development (CNPq) for supporting scientific equipment. L. C. A. Resende, L.A. Da Silva and J. P. Marchezi would like to thank the CBJLSW, NSSC and CAS for supporting their postdoctoral fellowships.

- Chang, L. C., Thayer, J. P., Lei, J., & Palo, S. (2009). Isolation of the global MLT thermal response to recurrent geomagnetic activity. *Geophysical Research Letters*, *36*, L15813. <https://doi.org/10.1029/2009gl039305>
- Chapman, S., & Lindzen, R. (1970). *Atmospheric tides. Thermal and gravitational*, D. Reidel.
- Clemesha, B. R., Takahashi, H., Simonich, D. M., Gobbi, D., & Batista, P. P. (2005). Experimental evidence for solar cycle and long-term changes in the low-latitude MLT region. *Journal of Atmospheric and Solar-Terrestrial Physics*, *67*, 191–196. [https://doi.org/10.1016/S1364-6826\(96\)00166-6](https://doi.org/10.1016/S1364-6826(96)00166-6)
- Da Silva, L. A., Satyamurty, P., Alves, L. R., Souza, V. M., Jauer, P. R., Silveira, M. V. D., et al. (2016). Comparison of geophysical patterns in the southern hemisphere mid-latitude region. *Advances in Space Research*, *58*(10), 2090–2103. <https://doi.org/10.1016/j.asr.2016.04.003>
- Da Silva, L. A., Shi, J., Alves, L. R., Sibeck, D., Marchezi, J. P., Medeiros, C., et al. (2021). High-energy electron flux enhancement pattern in the outer radiation belt in response to the Alfvénic fluctuations within high-speed solar wind stream: A statistical analysis. *Journal of Geophysical Research: Space Physics*, *126*. <https://doi.org/10.1029/2021JA029363>
- Da Silva, L. A., Shi, J., Alves, L. R., Sibeck, D., Souza, V. M., Marchezi, J. P., et al. (2021). Dynamic mechanisms associated with high-energy electron flux dropout in the Earth's outer radiation belt under the influence of a coronal mass ejection sheath region. *Journal of Geophysical Research: Space Physics*, *126*, e2020JA028492. <https://doi.org/10.1029/2020JA028492>
- Da Silva, L. A., Sibeck, D., Alves, L. R., Souza, V. M., Jauer, P. R., Claudepierre, S. G., et al. (2019). Contribution of ULF wave activity to the global recovery of the outer radiation belt during the passage of a high-speed solar wind stream observed in September 2014. *Journal of Geophysical Research: Space Physics*, *124*, 1660–1678. <https://doi.org/10.1029/2018JA026184>
- Deepa, V., Ramkumar, G., Antonita, M., & Kumar, K. K. (2008). Meteor wind radar observations of tidal amplitudes over a low-latitude station Trivandrum (8.51°N, 77.1°E): Inter-annual variability and the effect of background wind on diurnal tidal amplitudes. *Journal of Atmospheric and Solar-Terrestrial Physics*, *70*, 2005–2013. <https://doi.org/10.1016/j.jastp.2008.07.017>
- Dickinson, R. E. (1975). Solar variability and the lower atmosphere. *Bulletin of the American Meteorological Society*, *56*, 1240–1248. [https://doi.org/10.1175/1520-0477\(1975\)056<1240:svatla>2.0.co;2](https://doi.org/10.1175/1520-0477(1975)056<1240:svatla>2.0.co;2)
- Echer, E., Gonzalez, W. D., Tsurutani, B. T., & Gonzalez, A. L. C. (2008). Interplanetary conditions causing intense geomagnetic storms (Dst ≤ -100 nT) during solar cycle 23 (1996–2006). *Journal of Geophysical Research*, *113*, A05221. <https://doi.org/10.1029/2007JA012744>
- Emmert, J. T., & Picone, J. M. (2010). Climatology of globally averaged thermospheric mass density. *Journal of Geophysical Research*, *115*, A09326. <https://doi.org/10.1029/2010JA015298>
- Fleener, J. W., Taylor, S., & Chappelow, C. (2008). *Leveraging the impact of 360-degree feedback* (p. 334). John Wiley & Sons.
- Forbes, J. M. (1982a). Atmospheric tides: 1. Model description and results for the solar diurnal component. *Journal of Geophysical Research*, *87*, 5222–5240. <https://doi.org/10.1029/JA087iA07p05222>
- Forbes, J. M. (1982b). Atmospheric tides: 2. The solar and lunar semidiurnal components. *Journal of Geophysical Research*, *87*, 5241–5252. <https://doi.org/10.1029/JA087iA07p05241>
- Forbes, J. M., & Garret, H. B. (1979). Theoretical studies of atmospheric tides. *Reviews of Geophysics*, *17*, 1951–1981. <https://doi.org/10.1029/RG017i008p01951>
- Fritts, D. C., & Isler, J. R. (1994). Mean motions and tidal and two-day wave structure and variability in the mesosphere and lower thermosphere over Hawaii. *Journal of the Atmospheric Sciences*, *51*, 2145–2164. [https://doi.org/10.1175/1520-0469\(1994\)051<2145:mmatat>2.0.co;2](https://doi.org/10.1175/1520-0469(1994)051<2145:mmatat>2.0.co;2)
- Fuller-Rowell, T., & Rees, D. (1980). A three dimensional time dependent global model of the thermosphere. *Journal of the Atmospheric Sciences*, *37*, 2545–2567. [https://doi.org/10.1175/1520-0469\(1980\)037<2545:atddg>2.0.co;2](https://doi.org/10.1175/1520-0469(1980)037<2545:atddg>2.0.co;2)
- Fytterer, T., Santee, M. L., Sinnhuber, M., & Wang, S. (2015). The 27 day solar rotational effect on mesospheric nighttime OH and O3 observations induced by geomagnetic activity. *Journal of Geophysical Research: Space Physics*, *120*, 7926–7936. <https://doi.org/10.1002/2015JA021183>
- Gonzalez, W. D., Dutra, S. L. G., & Pinto, O. (1987). Middle atmospheric electrodynamic modification by particle precipitation at the South Atlantic Magnetic Anomaly. *Journal of Atmospheric and Solar-Terrestrial Physics*, *49*(4), 377–383. [https://doi.org/10.1016/0021-9169\(87\)90032-8](https://doi.org/10.1016/0021-9169(87)90032-8)
- Greisiger, K. M., Schminder, R., & Kuerschner, D. (1987). Long-period variations of wind parameters in the mesopause region and the solar cycle dependence. *Journal of Atmospheric and Solar-Terrestrial Physics*, *49*, 281–285. [https://doi.org/10.1016/0021-9169\(87\)90063-8](https://doi.org/10.1016/0021-9169(87)90063-8)
- Guharay, A., Batista, P. P., & Andrioli, V. F. (2019). Investigation of solar cycle dependence of the tides in the low latitude MLT using meteor radar observations. *Journal of Atmospheric and Solar-Terrestrial Physics*, *193*, 105083. <https://doi.org/10.1016/j.jastp.2019.105083>
- Guharay, A., Batista, P. P., & Clemesha, B. R. (2015). On the variability of the diurnal tide and coupling with planetary waves in the MLT over Cachoeira Paulista (22.7°S, 45°W). *Journal of Atmospheric and Solar-Terrestrial Physics*, *133*, 7–17. <https://doi.org/10.1016/j.jastp.2015.07.016>
- Gurubaran, S., & Rajaram, R. (1999). Long-term variability in the mesospheric tidal winds observed by MF radar over Tirunelveli (8.7°N, 77.8°E). *Geophysical Research Letters*, *26*, 113–116. <https://doi.org/10.1029/1999GL900171>
- Hagan, M. E., Burrage, M. D., Forbes, J. M., Hackney, J., Randel, W. J., & Zhang, X. (1999). GSWM-98: Results for migrating solar tides. *Journal of Geophysical Research*, *104*, 6813–6827. <https://doi.org/10.1029/1998JA900125>
- Hagan, M. E., & Forbes, J. M. (2002). Migrating diurnal tides in the upper atmosphere excited by tropospheric latent heat release. *Journal of Geophysical Research*, *107*, 475415. <https://doi.org/10.1029/2001JD001236>
- Hagan, M. E., & Forbes, J. M. (2003). Migrating and nonmigrating semidiurnal tides in the upper atmosphere excited by tropospheric latent heat release. *Journal of Geophysical Research*, *108*(A2), 1062. <https://doi.org/10.1029/2002JA009466>
- Hocking, W. K., Fuller, B., & Vandepier, B. (2001). Real-time determination of meteor-related parameters utilizing modern digital technology. *Journal of Atmospheric and Solar-Terrestrial Physics*, *63*(2–3), 155–169. [https://doi.org/10.1016/S1364-6826\(00\)00138-3](https://doi.org/10.1016/S1364-6826(00)00138-3)
- Hocking, W. K., & Thayaparan, T. (1997). Simultaneous and co-located observation of winds and tides by MF and Meteor radars over London, Canada, (43°N; 81°W) during 1994–1996. *Radio Science*, *32*, 833–865. <https://doi.org/10.1029/96RS03467>
- Holton, J. R., & Staley, D. O. (1973). An introduction to dynamic meteorology. *American Journal of Physics*, *41*, 752–754. <https://doi.org/10.1119/1.1987371>
- Huang, F. T., & Reber, C. A. (2003). Seasonal behavior of the semi-diurnal and diurnal tides, and mean flows at 95 km, based on measurements from the High Resolution Doppler Imager (HRDI) on the Upper Atmosphere Research Satellite (UARS). *Journal of Geophysical Research*, *108*(12), 4360. <https://doi.org/10.1029/2002JD003189>
- Imura, H., Fritts, D., & Riggins, D. M. (2010). Long-term oscillations of the wind field in the tropical mesosphere and lower thermosphere from Hawaii MF radar measurements. *Journal of Geophysical Research*, *115*. <https://doi.org/10.1029/2009JD012509>
- Jacobi, C. (1998). On the solar cycle dependence of winds and planetary waves as seen from mid-latitude D1 LF mesopause region wind measurements. *Annales Geophysicae*, *16*, 1534–1543. <https://doi.org/10.1007/s00585-998-1534-3>
- Jacobi, C., Schminder, R., Kürschner, D., Bremer, J., Greisiger, K. M., Hoffmann, P., & Singer, W. (1997). Long-term trends in the mesopause wind field obtained from LF D1 wind measurements at Collm, Germany. *Advances in Space Research*, *20*, 2085–2088. [https://doi.org/10.1016/S0273-1177\(97\)00599-1](https://doi.org/10.1016/S0273-1177(97)00599-1)

- Jamison, B., & Regal, R. (1979). The statistical significance of data from superposed epoch analyses. *Solar-Terrestrial Influences of Weather and Climate*. In B. M. McCormac, & T. A. Seliga (Eds.) *Proceedings of a symposium/workshop held at the Fawcett Center for tomorrow, The Ohio State University, Columbus, Ohio, 24–28 August, 1978* (Vol. 13, pp. 175–179). Springer (ISBN: 978-94-009-9428-7). https://doi.org/10.1007/978-94-009-9428-7_17
- Jones, M., Jr., Emmert, J. T., Drob, D. P., Picone, J. M., & Meier, R. R. (2018). Origins of the thermosphere-ionosphere semiannual oscillation: Reformulating the “thermospheric spoon” mechanism. *Journal of Geophysical Research: Space Physics*, *123*, 931–954. <https://doi.org/10.1002/2017JA024861>
- Jones, M., Jr., Emmert, J. T., Drob, D. P., & Siskind, D. E. (2017). Middle atmosphere dynamical sources of the semiannual oscillation in the thermosphere and ionosphere. *Geophysical Research Letters*, *44*, 12–21. <https://doi.org/10.1002/2016GL071741>
- Luo, J., Liu, H., & Xu, X. (2021). Sporadic E morphology based on COSMIC radio occultation data and its relationship with wind shear theory. *Earth Planets Space*, *73*, 212. <https://doi.org/10.1186/s40623-021-01550-w>
- Mathews, J. D., & Bekeny, F. S. (1979). Upper atmosphere tides and the vertical motion of ionospheric sporadic layers at Arecibo. *Journal of Geophysical Research*, *84*(A6), 2743–2750. <https://doi.org/10.1029/JA084iA06p02743>
- Miyoshi, Y., & Kataoka, R. (2005). Ring current ions and radiation belt electrons during geomagnetic storms driven by coronal mass ejections and corotating interaction regions. *Geophysical Research Letters*, *32*, L21105. <https://doi.org/10.1029/2005GL024590>
- Mohankumar, K. (1985). An investigation on the influence of solar cycle on mesospheric temperature. *Planetary and Space Science*, *33*, 795–805. [https://doi.org/10.1016/0032-0633\(85\)90033-9](https://doi.org/10.1016/0032-0633(85)90033-9)
- Mukhtarov, P., & Pancheva, D. (2012). Thermosphere-ionosphere coupling in response to recurrent geomagnetic activity. *Journal of Atmospheric and Solar-Terrestrial Physics*, *90–91*, 132–145. <https://doi.org/10.1016/j.jastp.2012.02.013>
- Murphy, K. R., Watt, C. E. J., Mann, I. R., Jonathan Rae, I., Sibeck, D. G., Boyd, A. J., et al. (2018). The global statistical response of the outer radiation belt during geomagnetic storms. *Geophysical Research Letters*, *45*(9), 3783–3792. <https://doi.org/10.1002/2017GL076674>
- Nakamura, T., Fritts, D. C., Isler, J. R., Tsuda, T., Vincent, R. A., & Reid, I. M. (1997). Short-period fluctuations of the diurnal tide observed with low-latitude MF and meteor radars during CADRE: Evidence for gravity wave/tidal interactions. *Journal of Geophysical Research*, *102*, 2625–26238. <https://doi.org/10.1029/96JD03145>
- Namboothiri, S. P., Manson, A. H., & Meek, C. E. (1993). Variations of mean winds and tides in the upper middle atmosphere over a solar cycle, Saskatoon, Canada, 52°N, 107°W. *Journal of Atmospheric and Solar-Terrestrial Physics*, *55*, 1325–1334. [https://doi.org/10.1016/0021-9169\(93\)90101-4](https://doi.org/10.1016/0021-9169(93)90101-4)
- Nishino, M., Makita, K., Yumoto, K., Miyoshi, Y., Schuch, N. J., & Abdu, M. A. (2006). Energetic particle precipitation in the Brazilian geomagnetic anomaly during the “Bastille Day storm” of July 2000. *Earth Planets Space*, *58*(5), 607–616. <https://doi.org/10.1186/bf03351958>
- Niu, J., Weng, L. B., Meng, X., & Fang, H. X. (2019). Morphology of ionospheric sporadic E layer intensity based on COSMIC occultation data in the midlatitude and low-latitude regions. *Journal of Geophysical Research: Space Physics*, *124*(6), 4796–4808. <https://doi.org/10.1029/2019JA026828>
- Oberheide, J., Forbes, J. M., Häusler, K., Wu, Q., & Bruinsma, S. L. (2009). Tropospheric tides from 80 to 400 km: Propagation, interannual variability, and solar cycle effects. *Journal of Geophysical Research*, *114*, D00105. <https://doi.org/10.1029/2009JD012388>
- Pancheva, D., Mitchell, N., Middleton, H. R., & Muller, H. G. (2003). Variability of the semidiurnal tide due to fluctuations in solar activity and total ozone. *Journal of Atmospheric and Solar-Terrestrial Physics*, *65*, 1–19. [https://doi.org/10.1016/S1364-6826\(02\)00084-6](https://doi.org/10.1016/S1364-6826(02)00084-6)
- Pezzopane, M., Pignalberi, A., & Pietrella, M. (2015). On the influence of solar activity on the mid-latitude sporadic E layer. *Journal of Space Weather and Space Climate*, *5*, A31. <https://doi.org/10.1051/swsc/2015031>
- Pinto, O., & Gonzalez, W. D. (1989). Energetic electron precipitation at the South Atlantic magnetic anomaly: A review. *Journal of Atmospheric and Solar-Terrestrial Physics*, *51*(5), 351–365. [https://doi.org/10.1016/0021-9169\(89\)90117-7](https://doi.org/10.1016/0021-9169(89)90117-7)
- Pinto, O., Gonzalez, W. D., & Gonzalez, A. (1989). Time variations of X Ray fluxes at the South Atlantic Magnetic Anomaly in association with a strong geomagnetic storm. *Journal of Geophysical Research*, *94*(A12), 17275–17280. <https://doi.org/10.1029/ja094ia12p17275>
- Ponomarev, E. A., Sedykh, P. A., & Urbanovich, V. D. (2006). Bow shock as a power source for magnetospheric processes. *Journal of Atmospheric and Solar-Terrestrial Physics*, *68*, 685–690. <https://doi.org/10.1016/j.jastp.2005.11.007>
- Reddi, C. R., & Ramkumar, G. (1997). Climatologies of tidal winds in the radio-meteor region over Trivandrum (81°N). *Journal of Atmospheric and Solar-Terrestrial Physics*, *59*, 1757–1777. [https://doi.org/10.1016/S1364-6826\(97\)00042-4](https://doi.org/10.1016/S1364-6826(97)00042-4)
- Reinisch, B. W., Galkin, I. A., Khmyrov, G. M., Kozlov, A. V., Bibl, K., Lisysyan, I. A., et al. (2009). New digisonde for research and monitoring applications. *Radio Science*, *44*, 1RS0A24. <https://doi.org/10.1029/2008RS004115>
- Resende, L. C. A., Batista, I. S., Denardini, C. M., Batista, P. P., Carrasco, A. J., Andrioli, V. F., & Moro, J. (2017a). The influence of tidal winds in the formation of blanketing sporadic E-layer over equatorial Brazilian region. *Journal of Atmospheric and Solar-Terrestrial Physics*, *171*, 64–71. <https://doi.org/10.1016/j.jastp.2017.06.009>
- Resende, L. C. A., Batista, I. S., Denardini, C. M., Batista, P. P., Carrasco, A. J., Andrioli, V. F., & Moro, J. (2017b). Simulations of blanketing sporadic E-layer over the Brazilian sector driven by tidal winds. *Journal of Atmospheric and Solar-Terrestrial Physics*, *154*, 104–114. <https://doi.org/10.1016/j.jastp.2016.12.012>
- Resende, L. C. A., Shi, J., Denardini, C. M., Batista, I. S., Nogueira, P. A. B., Arras, C., et al. (2020). The influence of disturbance dynamo electric field in the formation of strong sporadic E layers over Boa Vista, a low-latitude station in the American sector. *Journal of Geophysical Research*, *125*, e2019JA027519. <https://doi.org/10.1029/2019JA027519>
- Resende, L. C. A., Shi, J., Denardini, C. M., Batista, I. S., Picanço, G. A., Moro, J., et al. (2021). The impact of the disturbed electric field in the sporadic E (Es) layer development over Brazilian region. *Journal of Geophysical Research: Space Physics*, *126*, e2020JA028598. <https://doi.org/10.1029/2020JA028598>
- Richardson, I. G., & Cane, H. V. (2010). Near-earth interplanetary coronal mass ejections during solar cycle 23 (1996–2009): Catalog and summary of properties. *Solar Physics*, *264*(1), 189–237. <https://doi.org/10.1007/s11207-010-9568-6>
- Richardson, I. G., Webb, D. F., Zhang, J., Berdichevsky, D. B., Biesecker, D. A., Kasper, J. C., et al. (2006). Major geomagnetic storms (Dst ≤ -100 nT) generated by corotating interaction regions. *Journal of Geophysical Research*, *111*, A07S09. <https://doi.org/10.1029/2005JA011476>
- Scargle, J. D. (1982). Studies in astronomical time series analysis. II - statistical aspects of spectral analysis of unevenly spaced data. *Astrophysical Journal, Part 1*, *263*, 835–853. <https://doi.org/10.1086/160554>
- Schmidt, H., Brasseur, G. P., Charron, M., Manzini, E., Giorgetta, M. A., Diehl, T., et al. (2006). The HAMMONIA chemistry climate model: Sensitivity of the mesopause region to the 11-year solar cycle and CO₂ doubling. *Journal of Climate*, *19*, 3903–3931. <https://doi.org/10.1175/JCLI3829.1>
- Singh, D., & Gurubaran, S. (2017). Variability of diurnal tide in the MLT region over Tirunelveli (8.7°N), India: Consistency between ground- and space-based observations. *Journal of Geophysical Research: Atmospheres*, *122*, 2696–2713. <https://doi.org/10.1002/2016JD025910>

- Sprenger, K., & Schindler, R. (1969). Solar cycle dependence of winds in the lower ionosphere. *Journal of Atmospheric and Solar-Terrestrial Physics*, *31*, 217–221. [https://doi.org/10.1016/0021-9169\(69\)90100-7](https://doi.org/10.1016/0021-9169(69)90100-7)
- Sridharan, S., Tsuda, T., & Gurubaran, S. (2010). Long-term tendencies in the mesosphere/lower thermosphere mean winds and tides as observed by medium-frequency radar at Tirunelveli (8.7°N, 77.8°E). *Journal of Geophysical Research*, *115*, D08109. <https://doi.org/10.1029/2008JD011609>
- Stober, G., Matthias, V., Brown, P., & Chau, J. L. (2014). Neutral density variation from specular meteor echo observations spanning one solar cycle. *Geophysical Research Letters*, *41*, 6919–6925. <https://doi.org/10.1002/2014GL061273>
- Stone, E., Frandsen, A., Mewaldt, R. E., Christian, D., Margolies, J. F., Ormes, J. F., & Snow, F. (1998). The advanced composition explorer. *Space Science Reviews*, *86*(1/4), 1–22. <https://doi.org/10.1023/A:1005082526237>
- Thorne, R. M. (1980). The importance of energetic particle precipitation on the chemical composition of the middle atmosphere. *Pure and Applied Geophysics*, *118*(1), 128–151. <https://doi.org/10.1007/bf01586448>
- Tsurutani, B. T., & Gonzalez, W. D. (1997). *The interplanetary causes of magnetic storms: A review in Magnetic Storms. Geophysical Monographic Series* (Vol. 98, pp. 77–89). AGU. <https://doi.org/10.1029/GM098p0077>
- Tsurutani, B. T., Gonzalez, W. D., Gonzalez, A. L. C., Tang, F., Arballo, J. K., & Okada, M. (1995). Interplanetary origin of geomagnetic activity in the declining phase of the solar cycle. *Journal of Geophysical Research*, *100*(A11), 21717–21733. <https://doi.org/10.1029/95JA01476>
- Tsurutani, B. T., Hajra, R., Echer, E., & Lakhina, G. S. (2019). Comment on “First Observation of Mesosphere Response to the Solar Wind High-Speed Streams” by W. Yi et al. *Journal of Geophysical Research: Space Physics*, *124*, 8165–8168. <https://doi.org/10.1029/2018JA026447>
- Turner, D. L., Kilpua, E. K. J., Hietala, H., Claudepierre, S. G., O'Brien, T. P., Fennell, J. F., et al. (2019). The response of Earth's electron radiation belts to geomagnetic storms: Statistics from the Van Allen Probes era including effects from different storm drivers. *Journal of Geophysical Research*, *124*, 1013–1034. <https://doi.org/10.1029/2018JA026066>
- Turner, N. E., Mitchell, E. J., Knipp, D. J., & Emery, B. A. (2006). *Energetics of magnetic storms driven by corotating interaction regions: A study of geoeffectiveness in Recurrent magnetic storms. Geophysics Monographic Series* (Vol. 167, pp. 113–124). AGU. <https://doi.org/10.1029/167GM11>
- Turunen, E., Kero, A., Verronen, P. T., Miyoshi, Y., Oyama, S. I., & Saito, S. (2016). Mesospheric ozone destruction by high-energy electron precipitation associated with pulsating aurora. *Journal of Geophysical Research: Atmosphere*, *121*(11), 11852–11861. <https://doi.org/10.1002/2016JD025015>
- Vincent, R. A., Kovalam, S., Fritts, D. C., & Isler, J. R. (1998). Long-term MF radar observations of solar tides in the low-latitude mesosphere: Inter-annual variability and comparison with the GSWM. *Journal of Geophysical Research*, *103*, 8667–8683. <https://doi.org/10.1029/98JD00482>
- Whitehead, J. (1961). The formation of the sporadic-E in the temperate zones. *Journal of Atmospheric and Terrestrial Physics*, *20*(1), 1155–1167. [https://doi.org/10.1016/0021-9169\(61\)90097-6](https://doi.org/10.1016/0021-9169(61)90097-6)
- Yi, W., Reid, I. M., Xue, X., Younger, J. P., Murphy, D. J., Chen, T., & Dou, X. (2017). Response of neutral mesospheric density to geomagnetic forcing. *Geophysical Research Letters*, *44*, 8647–8655. <https://doi.org/10.1002/2017GL074813>
- Yi, W., Reid, I. M., Xue, X., Younger, J. P., Spargo, A. J., Murphy, D. J., et al. (2017). First observation of mesosphere response to the solar wind high-speed streams. *Journal of Geophysical Research*, *122*, 9080–9088. <https://doi.org/10.1002/2017JA024446>
- Zhang, Y. B., Wu, J., Guo, L. X., Hu, Y. L., Zhao, H. S., & Xu, T. (2015). Influence of solar and geomagnetic activity on sporadic-E layer over low, mid and high latitude stations. *Advances in Space Research*, *55*(5), 1366–1371. <https://doi.org/10.1016/j.asr.2014.12.010>
- Zuo, X. M., & Wan, W. X. (2002). The correlation between sporadic E-layers and solar activity. *Chinese Journal of Geophysics*, *45*(6), 759–765. <https://doi.org/10.1002/cjg2.295>